SAE The Engineering Resource For Advancing Mobility
400 COMMONWEALTH DRIVE WARRENDALE, PA 15096

# SAE Technical Paper Series

850494

# PLL Sensing for Engine Diagnostics and Control

**J. E. Morris**
EE/Watson School
SUNY-Binghamton, NY
**Thomas Chih-Chien Chen**
Dept. of Electrical Engineering
Purdue Univ.
West Lafayette, IN

Reprinted from SP-618—
Sensors and Actuators (1985)

International Congress
& Exposition
Detroit, Michigan
February 25 — March 1, 1985

850494

# PLL Sensing for Engine Diagnostics and Control

**J. E. Morris**
EE/Watson School
SUNY-Binghamton, NY
**Thomas Chih-Chien Chen**
Dept. of Electrical Engineering
Purdue Univ.
West Lafayette, IN

ABSTRACT

An electronic phase-lock loop system is described which acts as an FM demodulator to extract the combustion/compression acceleration/deceleration fluctuations in the angular crankshaft velocity from an optical encoder signal. Further processing can provide roughness detection with a second phase-lock loop, and other similarly useful engine control or diagnostic parameters.

IN MANY ENGINE CONTROL SYSTEMS, the parameter to be optimized (subject to other set constraints) is the output engine torque. Direct measurement is difficult, although some systems to do it have been described,(1-3) all using drive-shaft stress in some way. An alternative approach to monitoring engine performance is to test the combustion quality within the cylinder.(4-8) The intermediate parameter is the instantaneous acceleration/deceleration pattern at the flywheel due to the combustion/compression cycle of the internal combustion engine. Even at the flywheel, these fluctuations are not completely damped out by high inertia.(9,10) While there is more freedom available in the installation of suitable transducer systems during vehicle manufacture e.g. by including appropriate flywheel markings, retrofit installation is still feasible. An obvious technique is to monitor fluctuations in the time of passage of ring-gear teeth past a sensor (e.g. magnetic). The problem with this technique is that while the acceleration/deceleration pattern is clearly visible, it contains pseudo-noise due to tooth defects and irregularities introduced by the shrinking of the ring-gear on to the fly-wheel itself (e.g. figure 1). An alternative technique, especially for retrofit purposes, is to attach the sensor to the more accessible pulley-wheel at the front of the engine. In this case, the sensor could be a conventional optical encoder (figure 2) or any appropriate equivalent, which gives the true instantaneous angular position of the crankshaft.

The signal from such a sensor is a series of pulses of instantaneous frequency corresponding to instantaneous angular velocity. This signal can be regarded as a steady state carrier frequency corresponding to average rpm, frequency-modulated by the acceleration waveform. The extraction of the acceleration waveform therefore reduces to one of F.M. demodulation and, in principle, any of the conventional techniques could be used.

One apparently suited to digital/microprocessor technology is the timing of each incremental pulse, the storage of each time in RAM and subsequent computer analysis. In practice, this approach grossly overloads the microprocessor, or requires a second dedicated one. For 512-increment resolution (the most convenient better than the nominal 1 degree) at 6000 rpm, the timing system is storing away each reading in less than 20 $\mu$s. To detect 1% changes from the average (see figure 1) requires a 0.2 $\mu$s clock period (5MHz). These figures are close to practical on-board microcomputer limits and allow no margins. The system is quite feasible but requires a dedicated data-gathering system and then would still swamp a single control microcomputer with the volume of data to be analyzed.

There is an alternative approach which performs much of the preliminary data

*Numbers in parentheses designate references at end of paper.

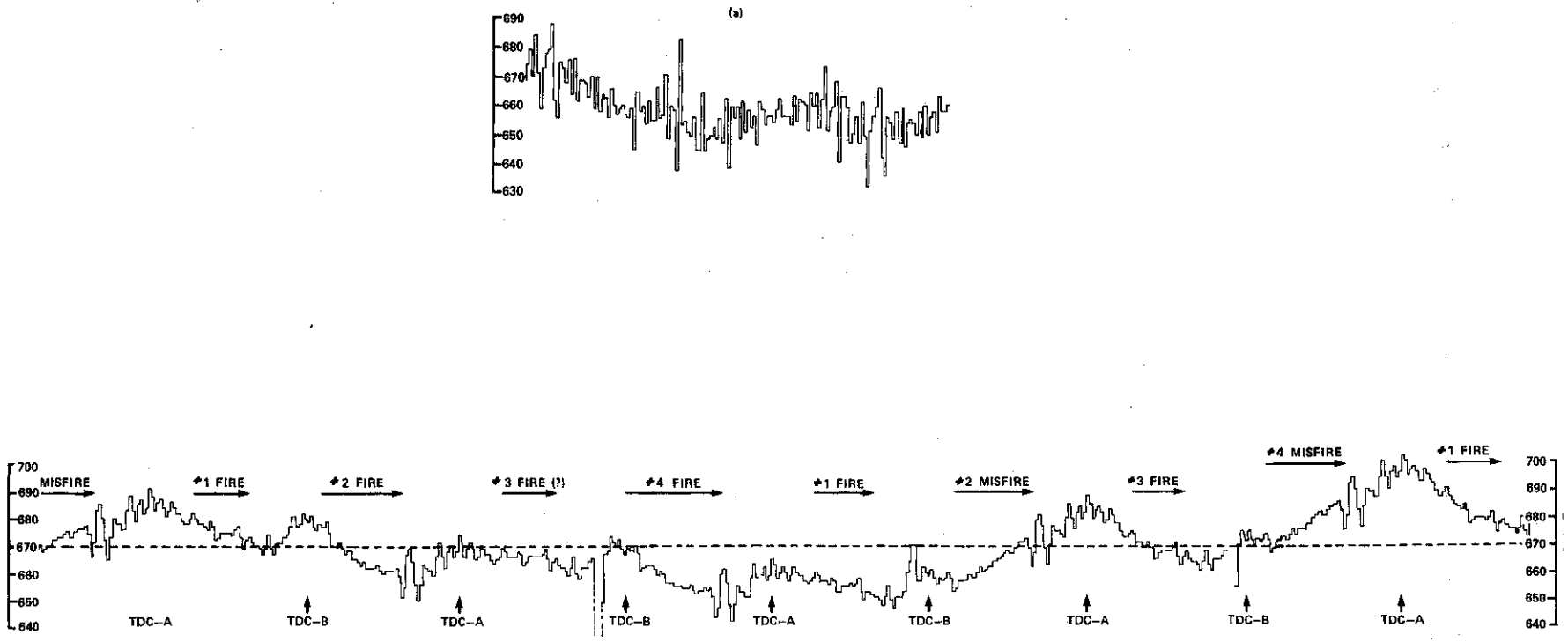


Figure 1. Times Between Successive Flywheel Teeth (μsec) At 960 RPM Idle
(a) 150 teeth, unsmoothed data
(b) 5 revolutions, 116 teeth/rev, data smoothed by Hanning filter

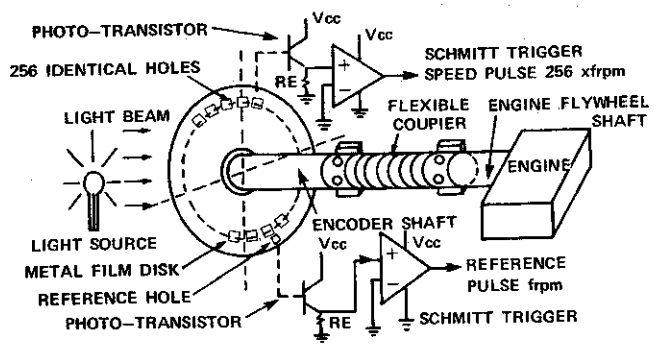


Figure 2. Schematic Diagram of the Optical Encoder

processing before going to the microcomputer. This technique uses a phase-lock loop (PLL), which is a common means of frequency demodulation nowadays, and provides some useful fringe benefits to either an on-board microcomputer engine control system or a more conventional diagnostic set-up as might be employed, for example, in a service center.

PHASE-LOCK LOOP REVIEW

The principle of the phase-lock loop is covered in a variety of modern electronics texts(11-15) and manufacturers' application notes.(16-18) Figure 3 shows the basic idea.

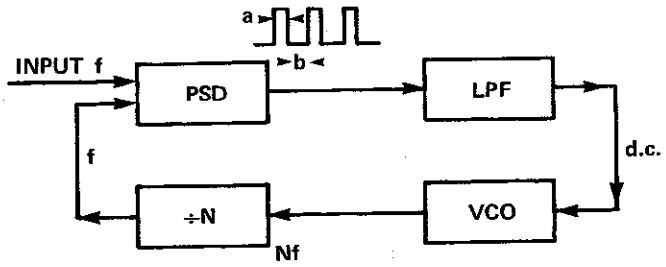


Figure 3. Basic PLL

The system input is a square wave of frequency f. Looking ahead a little, the second input to the phase-sensitive detector (PSD) is also a square-wave of frequency f, under steady-state conditions. The two inputs are slightly out of phase, leading to a pulse wave output from the PSD which is simply an exclusive-OR gate in its most elemental form. The mark-space ratio of the pulse wave is determined by the input phase difference and generates a proportional d.c. level at the output of the low-pass filter (LPF). This level ranges from zero for zero input phase difference to a maximum at 180 degrees, and determines the signal frequency Nf from the voltage-controlled oscillator (VCO). Nf may be divided down to f by the frequency divider (FD) where N can, of course, be 1. This frequency f is the second input we originally assumed at steady-state.

If the system input frequency f should vary to f + $\Delta$f, the output pulse width from the PSD will change, changing the VCO input level and its output to bring the feedback input frequency into line at f+ $\Delta$f. When a regular frequency modulation $f_m$ is superimposed upon the carrier $f_c$, the input $f = f_c + k \sin(2\pi f_m t)$ and the modulation signal $f_m$ is superimposed on the dc output from the LPF.

For transfer functions:

| | | |
|---|---|---|
| PSD: | $K_p$ | volts/rad |
| LPF: | $(1+s/\omega_o)^{-1}$ | for corner frequency $\omega_o/2\pi$ |
| VCO: | $K_v$ | rad/s-volt |
| FD: | $K_n$ | |

the open-loop forward gain is

$$G(s)= \Delta E(s)/\theta(s)=Kp(1+s/\omega_o)^{-1}$$

where $\Delta E$ is the d.c. output change for input phase difference $\theta$. The input parameter of interest, however, is the frequency variation $\Delta\omega(s)=s\theta(s)$, giving open-loop gain

$$G'(s)=\Delta E(s)/\Delta\omega(s)=K_p\, s^{-1}(1+s/\omega_o)^{-1}$$

The closed loop transfer function is then

$$H(s) = \Delta E(s)/\Delta\omega(s)$$
$$= G'(s)/(1+G'(s).K_v.K_n)$$
$$= K\omega_n^2/(s^2 + 2\zeta\omega_n s + \omega_n^2)$$

where $K = 1/(K_v K_n)$,

$\omega_n=(K_v K_n K_p \omega_o)^{1/2}$ -----natural frequency

$\zeta=0.5(\omega_o/K_v K_n K_p)^{1/2}$ ------damping ratio

and can be used to evaluate transient responses. Note that

$\omega_m < \omega_o < \omega_c$ for correct LPF operation.

EXPERIMENTAL

The optical encoder used was a 256 pulse per revolution (PPR) Encoder Products Co. model 712 (EPC-712) with the HD5 heavy duty option and positive reference pulse. 256 PPR rather than the intended 512 PPR brought the cost down a little and simplified some of the PLL system electronics. The HD5 option includes an external bearing to withstand 50lb. radial and 25lb. axial

loading factors. These were safety measures and may not have been necessary. A flexible coupler, in addition to the internal one, was inserted between the encoder and the crankshaft output. (figure 4)

All tests were run on a 1.6ℓ CVH 4-cylinder Ford Escort engine converted to single cylinder use by disabling the rear three cylinders. The rpm range was restricted by the engine set-up to 600 - 2100 rpm.

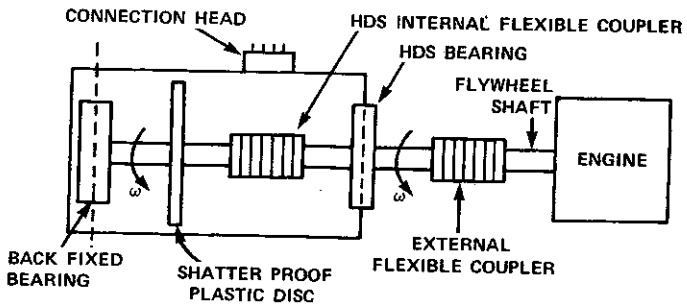


Figure 4. EPC 712-HD5 Optical Encoder

The PLL employed was the generic CMOS 4046 unit which includes two PSD's, the VCO and a d.c. output buffer on the VCO input. PSD1 offers superior noise rejection but narrow bandwidth; PSD2 reverses the trade-off. For engine applications, the 10:1 dynamic rpm range requires the wider bandwidth, and experimentally PSD2 provides better transient response off center-frequency.

BASIC ENGINE SENSOR

The system originally envisaged split the LPF into two stages: LPF1 and LPF2 (figure 5). In this idea, $\omega_m < \omega_1 < \omega_c$ but $\omega_1 < \omega_m$ so that the VCO input would be

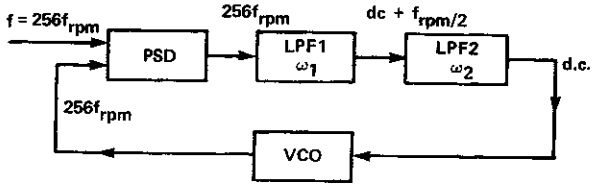


Figure 5. Block Diagram of PLL with Split LPF

constant during the steady-state engine cycle and the output would be taken from between LPF1 and LPF2. Unfortunately, the two-stage filter, of transfer function $(1+s/\omega_1)^{-1}(1+s/\omega_2)^{-1}$, introduces additional phase-shift into the feedback loop. Analysis shows that the stability requirements cannot be simultaneously met with the desired corner frequencies (Appendix A). The same condition pertains to second-order filters generally and a simple first-order LPF has therefore been used and found to be satisfactory.

We shall not go through the design procedures for each circuit of the overall system; these are outlined in detail elsewhere.(19) The final circuit design used to obtain the results presented below is shown in figure 6.

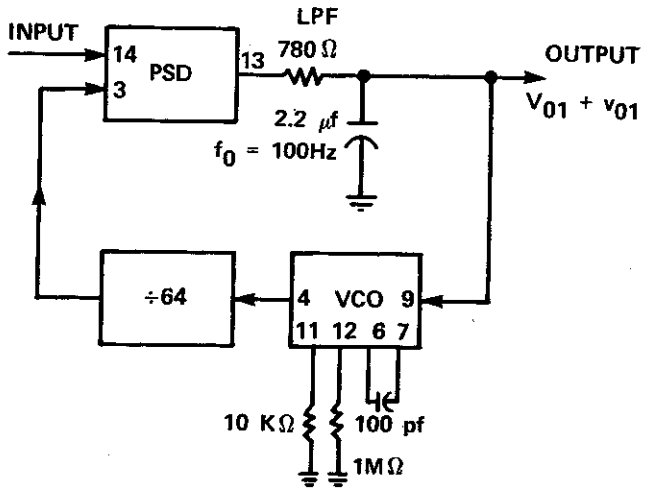


Figure 6. Circuit Diagram of PLL #1 showing 4046 pin numbers

The VCO test characteristics shown in figure 7 cover a linear range from 64 x 2.56 KHz, to 64 x 8.96 KHz, this being 64 x the input frequency range corresponding to 600 - 2100 rpm with the 256 increment encoder. The corresponding input voltage range is 2.5 to 6 volt, leaving room in a 12 volt system for higher rpm. The system will also work at lower rpm, but with increasing non-linearity in the output. One purpose of the ÷64 frequency divider will be explained below under Ancillary Signals; it also serves to lift the VCO operation well out of the non-linear low-frequency range.

The pulse-rate to the low-pass filter ranges from 2.56 to 8.96 KHz over the 600

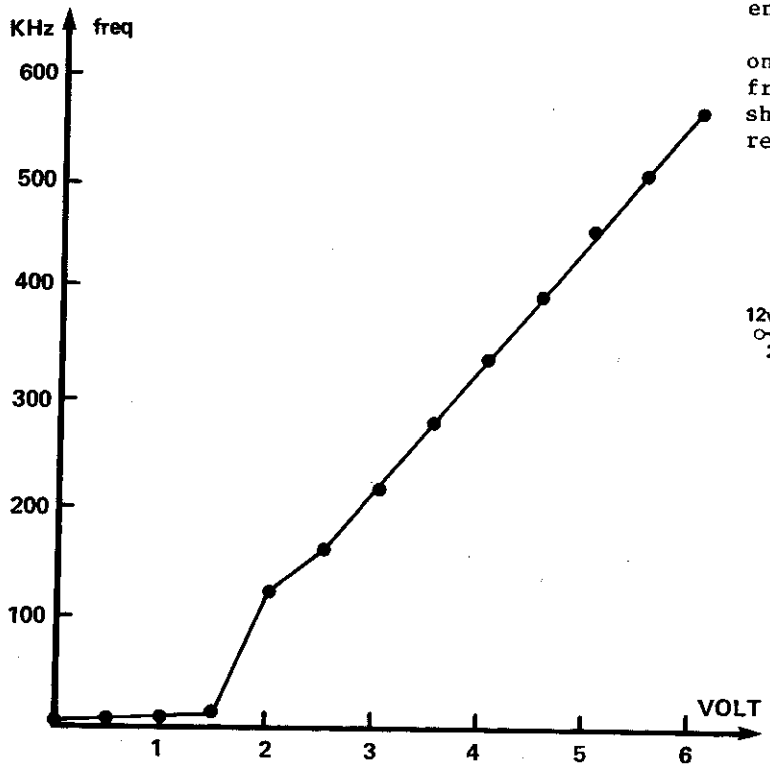


Figure 7. Voltage-Frequency Conversion of the 4046 VCO

to 2100 rpm range, while the acceleration/deceleration fluctuation frequency is 5.0 to 17.5 Hz for the single cycle engine (or n times this for an n-cylinder engine.) The cut-off frequency of an ideal LPF could be anywhere between 17.5 Hz and 2.56KHz to preserve the FM signal and reject the individual encoder pulses. In practice, however, it must be sufficiently high so that the maximum FM signal is not excessively phase-shifted (such that the acceleration peak posiition is moved, for example) but low enough that effective attenuation of the minimum encoder frequency is achieved. The corner frequency of the LPF employed is 100Hz, which produces a -9.9degree phase-shift at 17.5Hz and -28.2 dB attenuation (3.8% residual) at 2.56KHz. These figures provide an acceptable functional compromise, but one can still see the encoder frequency at the output and one would have to compensate later for the 10 degree shift in peak position, if that was a parameter of interest. As implied earlier, a second order filter improves high-frequency rejection but loses on increased phase shift. The design compromise would be tougher for a multicylinder engine but could be eased again by the use of a higher resolution encoder.

Sensor performance was first evaluated on the design bench, simulating the frequency-modulated encoder waveform as shown in figure 8. The modulating and recovered signals are compared in figure 9.

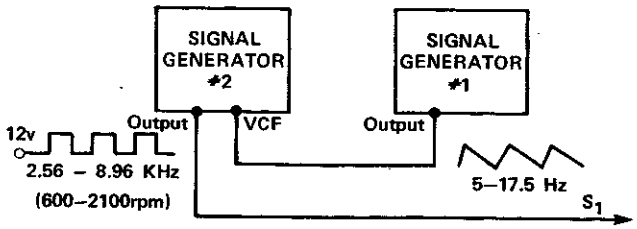


Figure 8. Laboratory Simulation of the Frequency-modulated (crankshaft) Input Signal

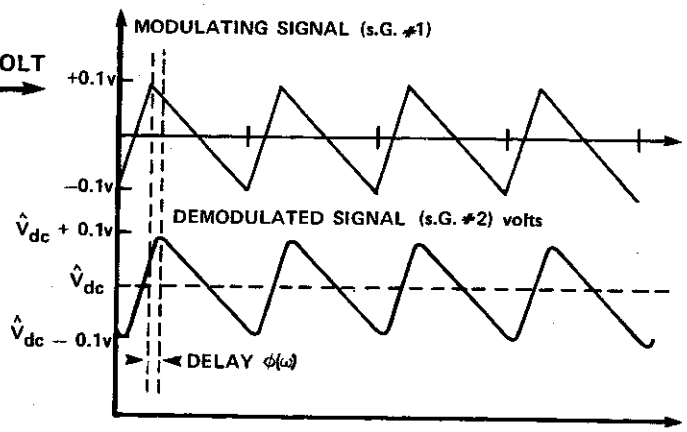


Figure 9. Modulation and Demodulation Signals of PLL#1

The $\pm$0.1 volt modulation produces $\pm$5% frequency variation. While the extraction is not perfect, the slight rounding of the corners due to high frequency roll-off is not a problem, effective attenuation being less than 0.13dB. The $\lesssim$10 degree phase shift, however, requires compensation in later processing.

Steady-state performance was also tested on the engine; least squares analysis of the dc component $V_{01}$ of the output voltage versus measured rpm showed that:

$$RPM = 100(V_{01} - 1.118)/0.229$$

i.e., it follows the intended 2.5-6 volts over the 600-2100 rpm range to within $\pm$1% error and linearity.

ROUGHNESS SENSING

The steady state output of the PLL #1, described above, contains both the d.c. component $V_{01}$ considered above, and the fluctuating a.c. acceleration signal. Under ideal running conditions, the frequency and amplitude of this a.c. component $v_{01}$ (figure 10) are constant. (Figures 10, 12, 15, 16, 19 and 21 have been traced from oscilloscope photographs.)

Figure 10. PLL #1 output $v_{01}$ (a) as is, and (b) after amplication and filtering (see $v_{01}$ figure 11)

(a)upper: 50 mv/div; (b)lower: 1.0 v/div H: 25 msec/div; At 1200 rpm

To achieve stoichiometric control with such a sensor, one must employ a dither technique. The intended fuel mixture control system, however, is for lean-limit operation based on roughness threshold sensing.(5,9,10,20-24) In this approach, the fuel mixture is steadily leaned-out until a roughness threshold is exceeded, whereupon the mixture is enriched by a set amount and the process repeats.

In such a system, a partial misfire (roughness) will produce a discontinuity in the repetitive output $v_{01}$ which can be regarded as an abrupt change of frequency. The discontinuity should be detectable using a second PLL #2 which also acts as an FM demodulator.

PLL #2 design principles are essentially the same as for PLL #1, but the 4046 input requires a 0 to 12 volt square wave which is produced from $V_{01} + v_{01}$ by the circuit of figure 11. The first LPF with corner frequency at 100Hz further eliminates undesirable high frequency noise in the input. The output of the second LPF (3Hz corner) contains both the dc and a reduced ac component of the input while that of the third LPF (1Hz corner) also contains the d.c. out but with negligible a.c. These last two are compared by the amplifier which converts the $\pm$0.1 volt $v_o$ to $\pm$2 volts, still with a d.c. offset which is removed at the comparator input. The bipolar output from the comparator is rectified (figure 12) and converted to a square wave by a simple flip-flop. The waveforms are shown schematically in figure 13.

Due to the ÷2 squaring operation, the (fundamental) input frequency to the roughness PLL is 2.5 to 8.75Hz. To keep the VCO within its linear frequency range, a frequency divider is used, this time with a 1024 ratio, setting the VCO frequency range from 2.56 to 8.96 KHz (1/64 times the

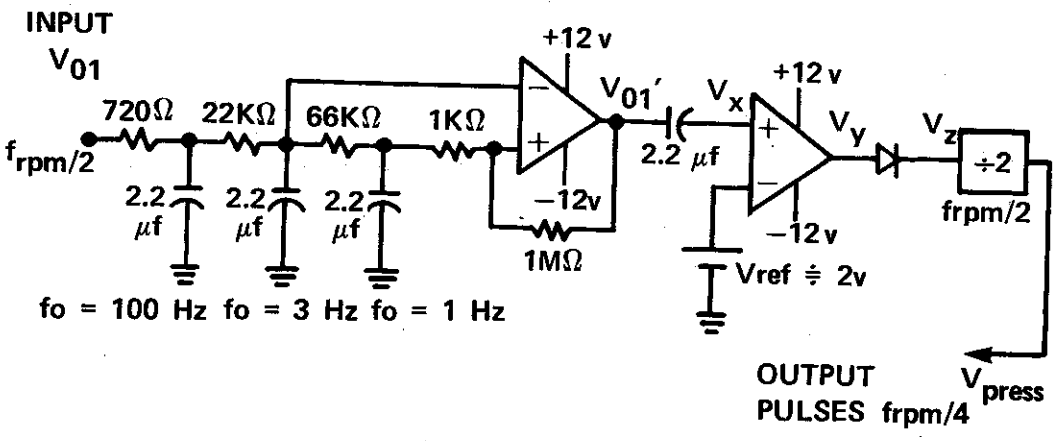


Figure 11. Amplification, filtering and conversion of $v_{01}$ to pulses for PLL #2

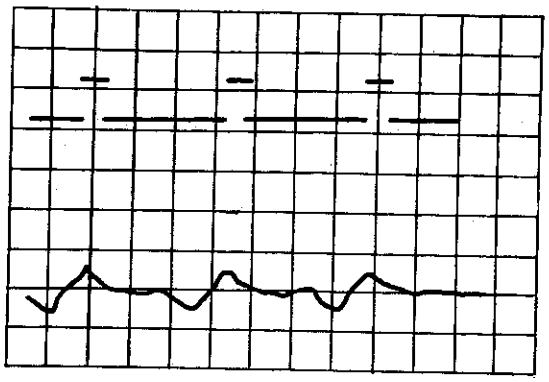

Figure 12. PLL #1 output interfacing to PLL #2 (roughness)--see figure 11--1800 rpm (Horizontal 25 msec/div)
(a) Upper trace: $v_z$ (Vertical 10v/div)
(b) Lower trace: $v_x$ (Vertical 4v/div)

basic VCO's frequency). The complete PLL #2 circuit is shown in figure 14.

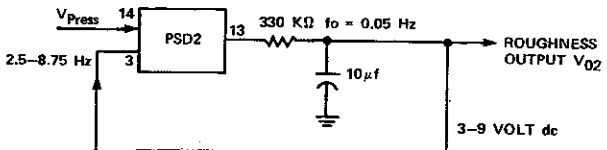


Figure 14. Circuit Diagram of PLL #2

The roughness detector output would normally be followed by some form of threshold detection, but this last step is specific to the control strategy and is not included here. Figure 15 shows a sequence of output signals from both PLL's to demonstrate the development of fluctuations in the steady state acceleration waveform $v_{01}$ (figure 15a) as the fuel mixture is weakened and the corresponding roughness PLL outputs $v_{02}$ (figure 15b). (Actually the waveforms in figure 15a are the amplified forms; see figures 12 and 13.)

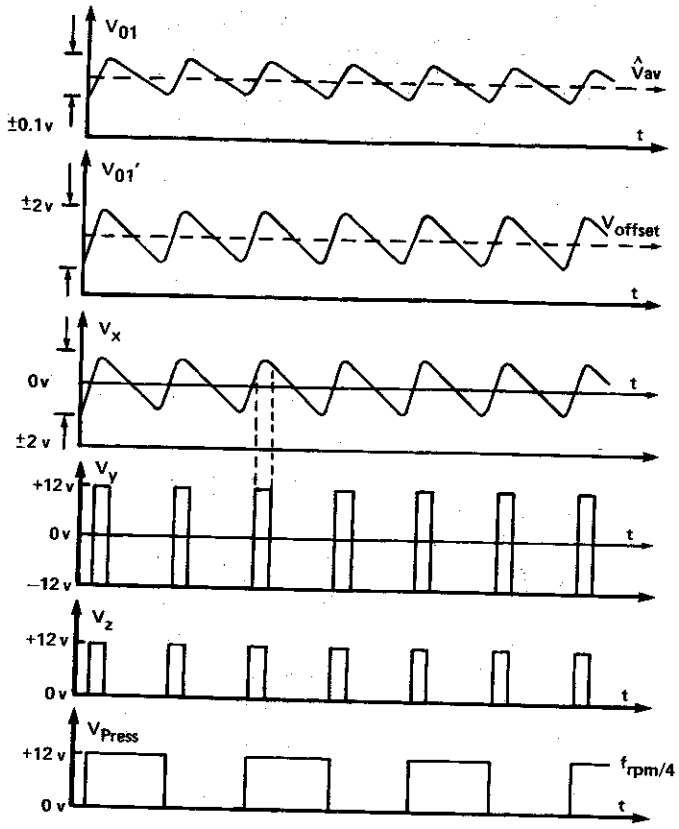


Figure 13. Circuit waveforms for figure 11

IGNITION TIMING CONTROLS

Just as timing may be controlled by determination of the combustion pressure peak position with compensating adjustment(5,10,25) an algorithm can be developed based upon the acceleration waveform and its peak position. For the latter case, the acceleration waveform is shown in figure 16 for various ignition angles with the reference marker pulse for comparison. It is relatively simple to send the reference pulse and one triggered by the peak signal to a microcontroller for timing information.

It is also possible to further unload the processor and provide the peak position in analog form, or possibly for an analog diagnostic display. A crude system to perform this task is shown in figure 17. Reference to figure 13 shows that the acceleration "peak" signal in this case is really only a rough approximation to this position, but the concept should be clear.

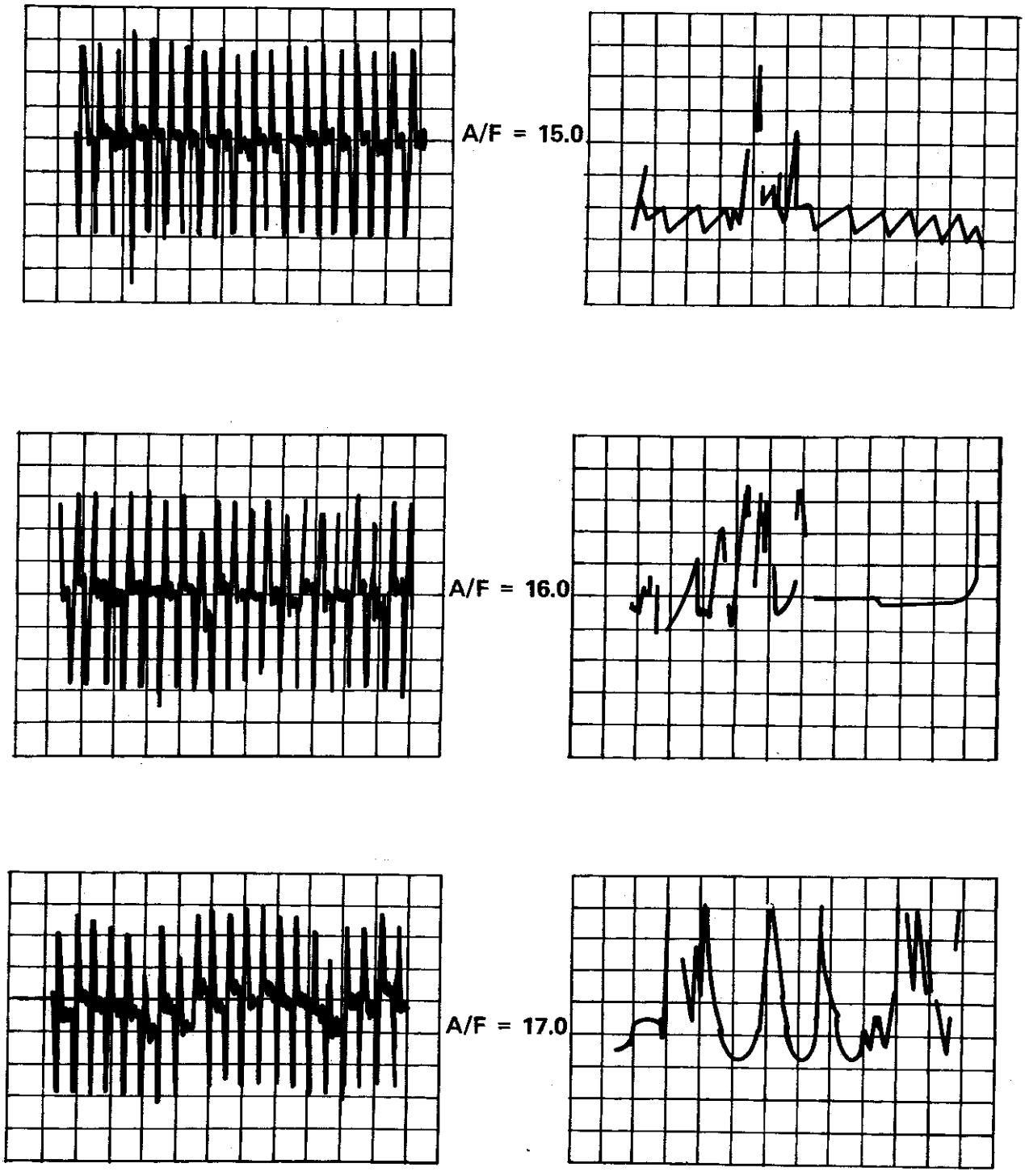


Figure 15. Variations of flywheel acceleration/deceleration signal and derived roughness with increasingly lean mixtures. (1200 rpm)

(a) Flywheel signal $v_{01}'$ derived from PLL #1
(0.25 sec/div horizontal)
(800 mV/div vertical)

(b) Roughness output from PLL #2, $v_{02}$
(1 sec/div horizontal)
(50 mV/div vertical)

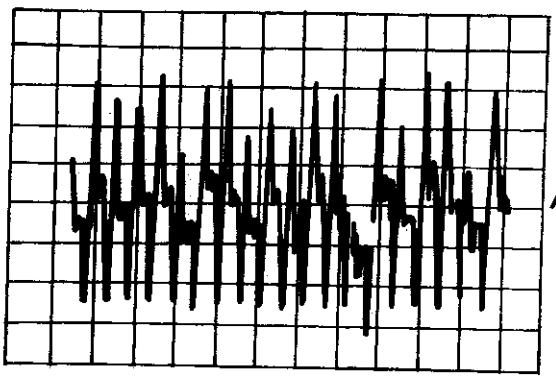

15 (a) continued

A/F = 18.0

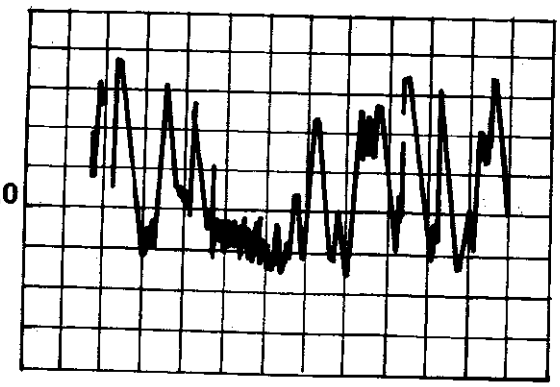

15 (b) continued

Figure 18 shows the acceleration peak position, as given by the d.c. output level of the detector system, as the firing angle is varied. The anomalous behavior at large advance angles is almost certainly due to the fact that the "peak position" signal used occurs before the true peak and deteriorates in accuracy as the acceleration waveform broadens, or smears out, with excessive advance.

Figure 19 shows the effect on the acceleration peak position (d.c. output) of switching from 30 degrees BTDC ignition through 20 degrees BTDC to 10 degrees BTDC.

ANCILLARY SIGNALS

(a) Microprocessor clock.

The advantages of using a microprocessor clock locked to engine rpm for control purposes have been described by Freimark.(26) In general, the need for time consuming multiplication and division is done away with since clock periods and crankshaft degrees are proportional at all rpm. The system proposed for this purpose was a PLL similar to PLL #1 described in the "Basic Engine Sensor" section above. In principle, the VCO output could be used to provide such an rpm-locked microprocessor clock with maximum frequency at 6000 rpm, say, of 64 x 25.6 KHz = 1.6 MHz. This frequency could be easily increased if needed by increasing the ÷64 ratio used.

(b) Real-time crank angle.

The 256-increment encoder output can be fed directly into an 8-bit counter to provide direct instantaneous readout of the true crankshaft angle (which does not vary linearly with time) for a microprocessor. The counter could interface directly to the data bus and would be more useful to a crystal-timed controller than to the rpm-locked system described above. It would be wise to provide a reset pulse from the encoder's reference marker to avoid cumulative errors.

(c) Acceleration/Deceleration Signal.

The d.c. output $V_{01}$ of the base PLL #1 represents engine rpm. In many control applications, engine acceleration or deceleration is a useful input to assist in the interpretation of other data, and acceleration/deceleration signals can be easily obtained by differentiation of the PLL #1 rpm output. For microprocessor control, some threshold may be appropriate before an input is triggered. For diagnostic displays, an analog reading may be appropriate, or perhaps A to D conversion for a dashboard display.

A suitable differentiator is shown in figure 20, comprised of high-pass and low-pass sections with identical corner frequencies. The circuit differentiates frequencies below 1Hz (also blocking the d.c. component) and attenuates (integrates) those above for noise reduction and elimination of engine rpm (5 to 17.5 Hz).

Experimental examples of the acceleration/deceleration circuit operation are shown in figure 21, where $\pm$25mV corresponds roughly to $\pm$100 rpm/sec.

CONCLUSIONS AND FUTURE WORK

The PLL #1 system described is the kernel of a versatile engine performance sensor which can be used for convenient visual analog displays, diagnostic systems or reduction of the pre-processing load for microprocessor controllers. Not only are the rotational acceleration/deceleration "fluctuations" of the crankshaft due to the combustion/compression cycle decoded, but ancillary processing can provide

1) roughness detection (with a second PLL #2)
2) "fluctuation" or combustion acceleration peak position
3) overall engine acceleration
4) real-time crank angle and
5) an rpm-locked microprocessor clock

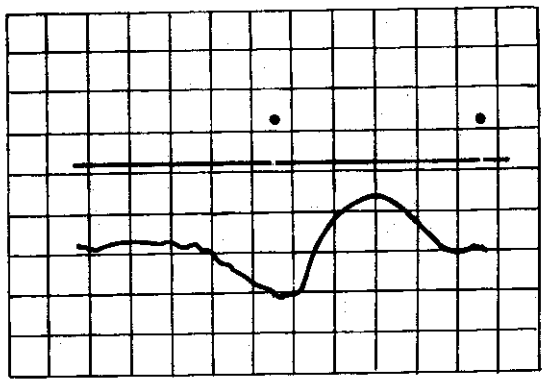

0° BTDC

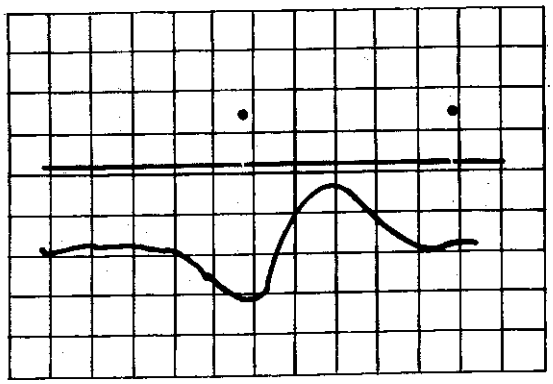

10° BTDC

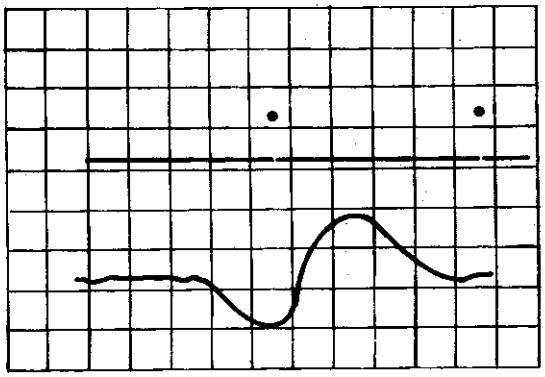

20° BTDC

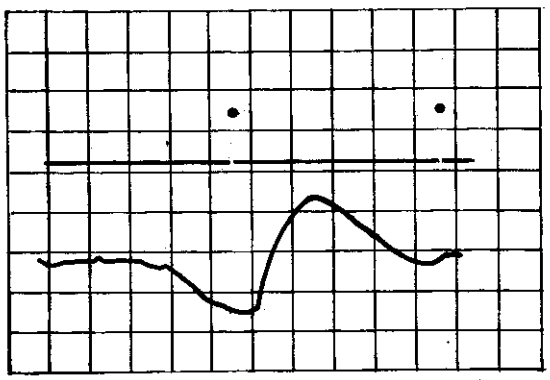

30° BTDC

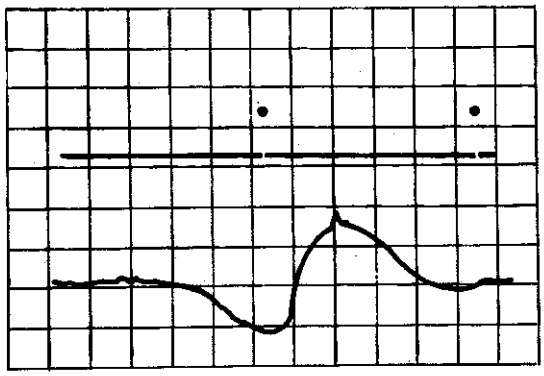

40° BTDC

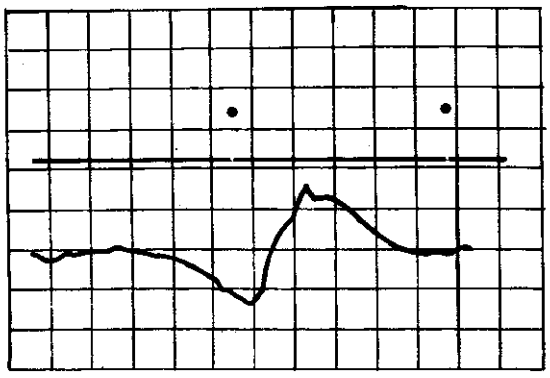

50° BTDC

Figure 16. Acceleration and deceleration of crankshaft: variation with ignition timing (1200 rpm, 12 msec/div horiz)
Upper trace: encoder reference pulse (10v/div)
Lower trace: $v_{01}'$ (1.6 v/div)

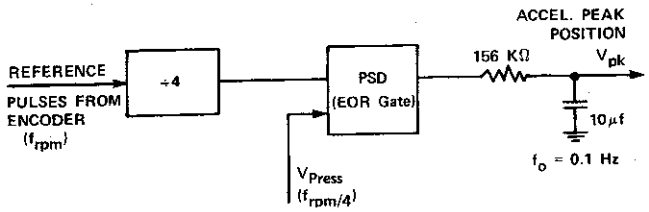


Figure 17. Crankshaft acceleration peak position determination relative to encoder reference ($V_{press}$: see figures 11 and 13)

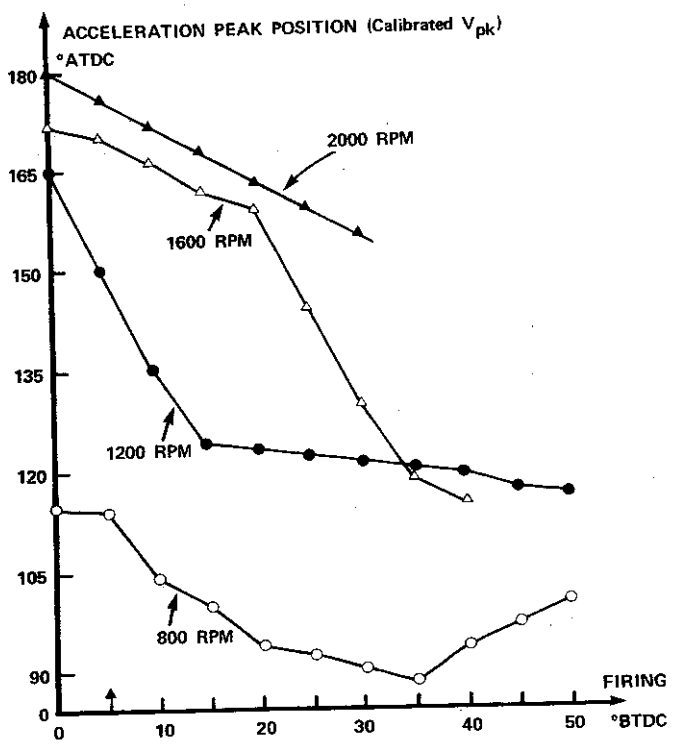


Figure 18. Acceleration peak position variations with ignition timing and rpm

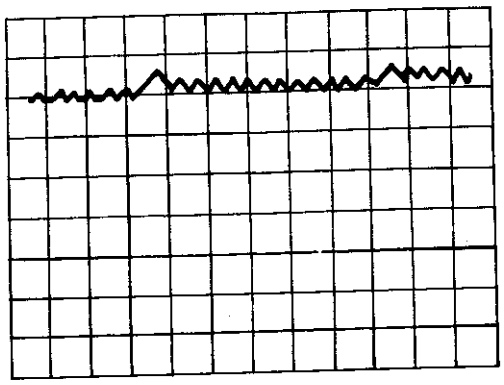

Figure 19. Variation in the acceleration detector output as ignition point is successively changed from 30 degrees BTDC to 20 degrees BTDC to 10 degrees BTDC. (Vert: 3v/div; horiz: 1sec/div)

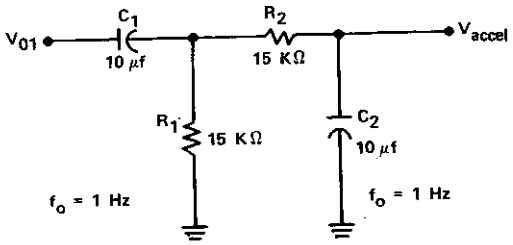


Figure 20. Differentiation circuit for longer-term engine acceleration/deceleration detection

The specific circuitry has been found to function adequately on the static single-cylinder test engine; the next steps are to extend the rpm range, adapt to multi-cylinder engines, test (diagnostic displays) on the road and incorporate the system into a control loop. For commercial implementation, the reliability limits of the encoder must be tested to bring the cost of that component down. A commercial unit would also be incorporated into the encoder housing, possibly as a thick-film hybrid in the prototyping stages.

In principle, the system would adapt directly to a diesel engine; in practice, the interpretation of the acceleration waveforms may be less straightforward than for spark-ignition. This step is certainly expected.

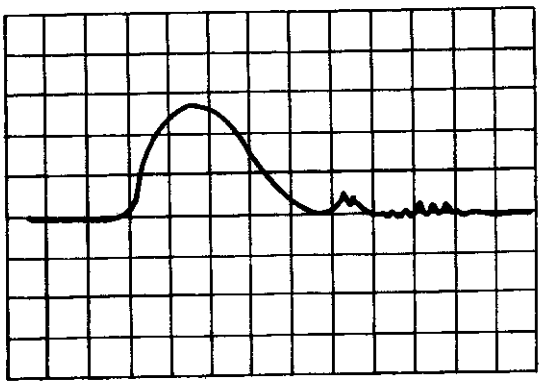

(a) ACCELERATION

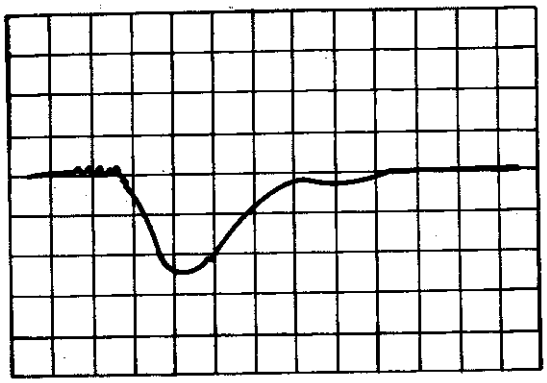

(b) DECELERATION

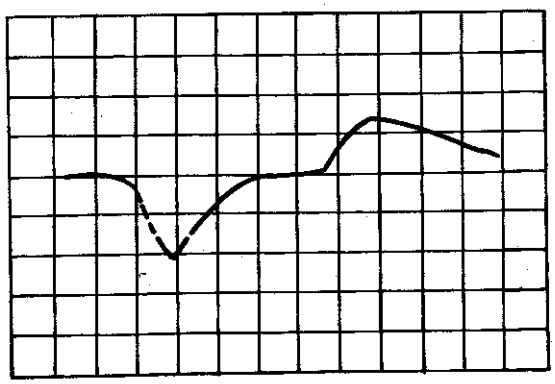

(c) DECELERATION & ACCELERATION

Figure 21. Sample outputs Vaccel from the acceleration circuit
(Vert: 60mV/div; horiz: 1sec/div)

ACKNOWLEDGEMENTS

This work was performed at the S.D. School of Mines and Technology as part of the MSEE requirements.(19) The authors are indebted to Dr. Dan Dolan and the Department of Mechanical Engineering for access to the test engine, use of equipment, advice, encouragement and their enthusiasm for the project.

## APPENDIX A
## Stability Analysis for Split LPF

In the system of figure A1, LPF1 must pass the maximum FM frequency 17.5 Hz but reject the minimum encoder frequency 2.56 KHz (i.e. meet the same design criteria outlined under Basic Engine Sensor) while LPF2 must also reject the 17.5 Hz, i.e.

$$35\pi << \omega_1 << 5120\pi, \quad \omega_2 << 35\pi$$

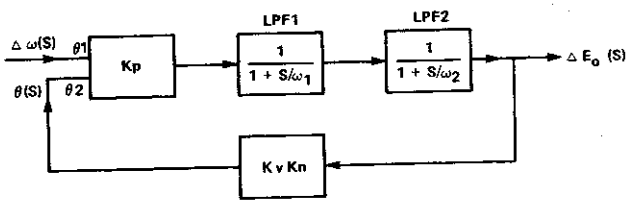


Figure A1. PLL #1 with split LPF: stability model

The closed loop system gain of the double-filter system is H'(s) =

$$\frac{K_p \omega_1 \omega_2}{s^3 + (\omega_1 + \omega_2)s^2 + \omega_1\omega_2 s + K_p K_v K_n \omega_1\omega_2}$$

The Routh coefficient array is:

| | |
|---|---|
| $1$ | $\omega_1\omega_2$ |
| $\omega_1 + \omega_2$ | $K_p K_v K_n \omega_1\omega_2$ |
| $\frac{(\omega_1 + \omega_2)\omega_1\omega_2 - K_p K_v K_n \omega_1\omega_2}{\omega_1 + \omega_2}$ | $0$ |
| $K_p K_v K_n \omega_1\omega_2$ | $0$ |

and for all parameters $\omega_1$, $\omega_2$, $K_p$, $K_n$ and $K_v$ positive, the Routh stability criterion for the closed-loop system reduces to:

$$\omega_1 + \omega_2 > K_p K_v K_n$$

But for the system described above (Basic Engine Sensor), $K_p K_v K_n = 24 \times 6400/3.5$ (Appendix B) which is totally inconsistent with the functional requirement of $\omega_1 << 5120\pi$.

The two requirements can be stated more generally for an N-increment encoder, as

$\omega_1 << 20N\pi$ and

$\omega_1 \ (\doteq \omega_1 + \omega_2) > (24/3.5)(2100-600)(10N/600)$

which should indicate more clearly that not even reducing N can cure the stability problem.

## APPENDIX B
## PLL Sensor Transient Response

For the purposes of theoretical estimation of the sensor's response time, it is necessary to evaluate the transfer function of each system element.

$K_p$ can be seen from figure A2 for a 12 volt exclusive-OR, to be $12/\pi$ volt/radian.

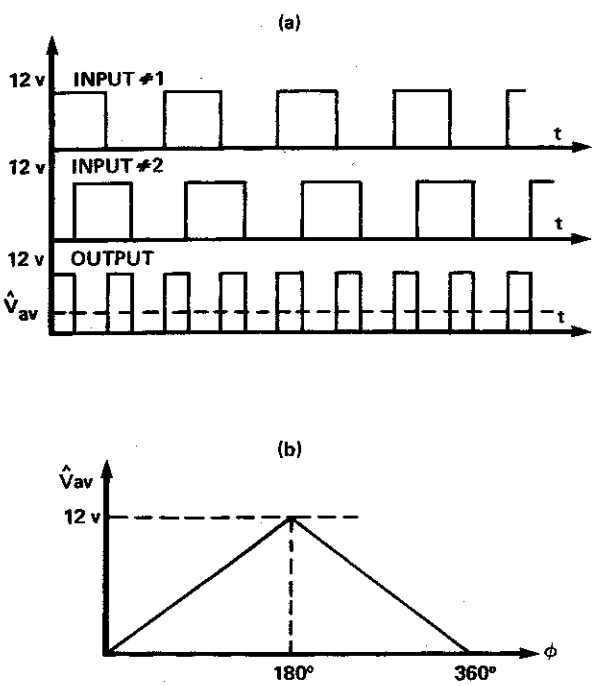


Figure A2. Exclusive OR Gate PSD

Similarly, $K_v$ from figure 7 is 64 x (8960-2560)/(6.0-2.5) Hz/volt = 64 x 6400 x $2\pi$/3.5 radians/sec-volt. $K_n$ is obviously 1/64 and $\omega_o = 200\pi$ rad/sec. The transfer function (PLL Review) is

$$H(s) = K\omega_n^2/(s^2 + 2\zeta\omega_n s + \omega_n^2)$$

where $K = 8.72 \times 10^{-5}$, $\omega_n = 5247.1$ and $\zeta = 0.06$. The transient response of interest is the degree to which the sensor output can track a steadily accelerating engine to provide accurate information to a microcomputer control or diagnostic system. 600 and 2100 rpm correspond roughly to 0(idle) and 35 mph and a maximum acceleration rate of 35 mph/sec is assumed (being more than twice that of the Porsche 911 Carrera!)(27)

For $\Delta\omega(t) = 2\pi \times 6400t$,

$E(t) = 3.5(t + A(t) + B(t) + C_3)$ where

$A(t) = C_1 (C_2 \sin\omega_d t + \cos\omega_d t) \exp -\zeta\omega_n t$

$B(t) = \omega_d^{-1} (C_2 \cos\omega_d t - \sin\omega_d t) \exp -\zeta\omega_n t$

and $C_1 = \zeta/\omega_n$

$C_2 = \zeta(1 - \zeta^2)^{1/2}$

$C_3 = -\zeta(2 - \zeta^2)/\omega_d$

$\omega_d = \omega_n(1 - \zeta^2)^{1/2}$

The calculated transient outputs completely track the ramp input within computer printout accuracy (see table A1) at the rate of 3.5 volts/sec for the input frequency shift corresponding to rpm: 600 + (2100-600)t. Any deviation from experimental steady state values is entirely attributable to experimental errors in the latter.

REFERENCES


1. A. Hergerich and J. Grupczynski "Capsule Torque - Meter Development" SAE paper 760746
2. G. Pratt "An Opto-electronic Torque Meter for Engine Control" SAE paper 760070
3. W. J. Fleming and P. W. Wood "Noncontact Miniature Torque Sensor for Automotive Application" SAE paper 820206
4. E. F. Obert "Internal Combustion Engines and Air Pollution" (3rd Ed.) Harper and Row pp 533-540
5. J. E. Morris, H. Anderson and R. Smith "Retrofit Feedback Control of A/F Ratio and Ignition Timing for Fuel Economy" SAE paper 820389 in "Electronic Engine Management and Driveline Controls" SAE publication P-104
6. J. E. Morris and Li-Chi, "Improved Intracylinder Pressure Sensing", SAE Paper 85 , SAE Congress, Detroit, 1985